Uptake of ^{18}F-Fluorocholine, ^{18}F-FET, and ^{18}F-FDG in C6 Gliomas and Correlation with ^{131}I-SIP(L19), a Marker of Angiogenesis

Matthias T. Wyss*[1], Nicolas Spaeth*[1], Gregoire Biollaz[2], Jens Pahnke[3,4], Patrizia Alessi[5], Eveline Trachsel[5], Valerie Treyer[1], Bruno Weber[1,6], Dario Neri[5], and Alfred Buck[1]

[1]PET Center, Division of Nuclear Medicine, University Hospital Zurich, Zurich, Switzerland; [2]Section of Clinical Immunology, University Hospital Zurich, Zurich, Switzerland; [3]Department of Pathology, University Hospital Zurich, Zurich, Switzerland; [4]Department of Neurology, University Rostock, Rostock, Germany; [5]Department of Applied Biosciences, Swiss Federal Institute of Technology, Zurich, Switzerland; and [6]Institute of Pharmacology and Toxicology, University Zurich, Zurich, Switzerland

Targeting extracellular structures that are involved in angiogenic processes, such as the extra domain B of fibronectin, is a promising approach for the diagnosis of solid tumors. The aim of this study was to determine uptake of the ^{18}F-labeled PET tracers ^{18}F-fluorocholine (*N,N*-dimethyl-*N*-^{18}F-fluoromethyl-2-hydroxyethylammonium), ^{18}F-fluoro-ethyl-L-tyrosine (FET), and ^{18}F-FDG in C6 gliomas of the rat and to correlate it with uptake of the anti–extra domain B antibody ^{131}I-SIP(L19) as a marker of neoangiogenesis. **Methods:** C6 gliomas were orthotopically induced in 17 rats. Uptake of all tracers was measured using quantitative autoradiography, and uptake of ^{18}F-fluorocholine, ^{18}F-FET, and ^{18}F-FDG was correlated with uptake of ^{131}I-SIP(L19) on a pixelwise basis. **Results:** The mean ^{131}I-SIP(L19), ^{18}F-fluorocholine, ^{18}F-FET, and ^{18}F-FDG standardized uptake values in the tumor and the contralateral normal cortex (in parentheses) were 0.31 ± 0.22 (not detectable), 2.00 ± 0.53 (0.49 ± 0.07), 3.67 ± 0.36 (1.42 ± 0.22), and 7.23 ± 1.22 (3.64 ± 0.51), respectively. The ^{131}I-SIP(L19) uptake pattern correlated best with ^{18}F-fluorocholine uptake ($\dot{z} = 0.80$, averaged $\dot{z}$-transformed Pearson correlation coefficient) and ^{18}F-FET uptake ($\dot{z} = 0.79$) and least with ^{18}F-FDG ($\dot{z} = 0.37$). **Conclusion:** One day after intravenous injection, ^{131}I-SIP(L19) displayed a very high tumor-to-cortex ratio, which may be used in the diagnostic work-up of brain tumor patients. Of the 3 investigated ^{18}F tracers, ^{18}F-fluorocholine and ^{18}F-FET correlated better with the pattern of ^{131}I-SIP(L19) uptake than did ^{18}F-FDG. Whether this means that ^{18}F-fluorocholine and ^{18}F-FET are better suited than ^{18}F-FDG to monitor antiangiogenic therapy should be investigated in future studies.

Key Words: extra domain B of fibronectin; angiogenesis; ^{18}F-fluorocholine; ^{18}F-fluoro-ethyl-L-tyrosine; ^{18}F-FDG

J Nucl Med 2007; 48:608–614
DOI: 10.2967/jnumed.106.036251

Vascular targeting and antiangiogenic strategies have been propagated as promising tools for diagnostic and therapeutic purposes (*1*). Angiogenesis, the development of new blood vessels from preexisting ones, is a typical feature of many malignant tumors and of benign disorders such as arthritis, diabetic retinopathy, and several others. The fact that tumor growth depends mainly on blood supply from newly built vessels (*2*) leads to the investigation of angiogenic markers. Today, the extra domain B of fibronectin is one of the most promising (*3*). It is present in the perivascular space of many aggressive solid tumors but not in normal tissue (except the ovaries and the endometrium). Extra domain B is identical in sequence in different species including rat, mouse, and man and has been successfully targeted with anti–extra domain B antibodies including the human recombinant antibody fragment scFv(L19) (*4*). In recent years, various L19 formats have been labeled with radioisotopes such as ^{123}I and ^{125}I for quantitative biodistribution analysis in murine tumor models and for immunoscintigraphic SPECT imaging of cancer patients (*5–7*). In accordance with the results of an immunohistochemical analysis of high- and low-grade astrocytomas (*8*), a study of Santimaria et al. (*6*) indicated a promising potential for radiolabeled L19 antibodies for diagnosis, grading, and therapy of human glioma patients.

In neurooncology, ^{18}F-FDG and ^{18}F-fluoro-ethyl-L-tyrosine (FET) are established tracers. ^{18}F-FET has the advantage of displaying a higher tumor-to-background ratio and of not accumulating in inflammatory lesions (*9,10*). On the other hand, ^{18}F-FDG is more widely available. The value of ^{18}F-fluorocholine in the evaluation of brain tumors is yet less clear, although a high tumor-to-background ratio has been demonstrated (*11*).

In a previous study, we showed that microvascular density influences the uptake of ^{18}F-fluorocholine but not of ^{18}F-FET or ^{18}F-FDG (*10*). The purpose of the present study was to correlate the uptake of ^{18}F-fluorocholine,

Received Sep. 4, 2006; revision accepted Dec. 15, 2006.
For correspondence or reprints contact: Alfred Buck, MD, Nuclear Medicine University Hospital, Rämistrasse 100, 8091 Zürich, Switzerland.
E-mail: fred.buck@usz.ch
*Contributed equally to this work.

^{18}F-FET, and ^{18}F-FDG with that of ^{131}I-SIP(L19) and therefore with the degree of neoangiogenesis. We hypothesized that a correlation of ^{18}F uptake with ^{131}I-SIP(L19) could point to a possible use of the ^{18}F tracer for the monitoring of antiangiogenic therapy warranting further studies in this field.

MATERIALS AND METHODS

Animals

Seventeen male Wistar rats weighing 250–350 g were used in this study. The experiments were approved by the local veterinary authorities. All animal work was performed by licensed investigators.

Radiopharmaceuticals

^{18}F-Labeled Tracers. ^{18}F-FDG was obtained from the commercial ^{18}F-FDG production of the University Hospital Zurich. The production of ^{18}F-FET and ^{18}F-fluorocholine was described in detail elsewhere (*12*).

^{131}I-SIP(L19). The SIP(L19) antibody was prepared according to a published procedure (*5*). The carrier-free radionuclide ^{131}I (98.0% radiochemical purity, 99% radionuclidic purity, with a specific activity of 675 GBq/mg) was obtained from Perkins Elmer as a solution of Na^{131}I in 0.1 M NaOH. The protein was radioiodinated using a modified chloramine-T labeling procedure in a ventilated hood. Typically, the antibody solution (200 μL, 100 μg of protein, 1.25×10^{-9} mol) was introduced into the vial with the starting Na^{131}I solution (10 μL) with 370 MBq (10 mCi, 3.56×10^{-9} mol of Na^{131}I) for the autoradiography experiments. Then, 5 μL of 0.5% aqueous solution of chloramine-T (25 μg, 1.17×10^{-7} mol) were added, and after 5 min at room temperature, the mixture was introduced into a Sephadex G-25 column (PD-10, GE Healthcare) previously treated with 1 mL of a 2% aqueous solution of bovine serum albumin for occupation of the nonspecific binding sites followed by equilibration with 25 mL of phosphate-buffered saline (pH 7.4). The column was eluted with phosphate-buffered saline. Fractions of 1 mL were collected. The labeled antibody was eluted from the column usually within the second or third fraction, whereas the unreacted ^{131}I remained at the column.

The labeling efficiency was usually about 75%, giving radioiodinated antibodies with specific activities of 222 GBq/μmol.

Cell Culture

The rat glioma cell line C6 was kindly provided by W. Risau (Bad Nauheim, Germany). C6 rat glioma cells were grown in Dulbecco's modified Eagle medium containing 4,500 mg of D-glucose (GIBCO, Life Technologies) per liter, supplemented with 10% fetal calf serum, 2 mM *N*-acetyl-L-alanyl-L-glutamine (Biochrom AG), and 20 μg of gentamycin (Sigma-Aldrich) per milliliter. For injection, the cells were harvested by trypsinization, washed 3 times with phosphate-buffered saline, and resuspended at a final concentration of 10^8 cells/mL.

Inoculation Procedure

The rats were anesthetized with an intraperitoneal injection of a mixture of ketamine (50 mg/kg; Ketasol 100, Dr. E. Graeub AG) and medetomidine (1 mg/kg; Domitor, Dr. E. Graeub AG) and placed in a stereotactic frame (David Kopf Instruments). We used the inoculation method of Ambar et al. with few modifications (*13*). After preparation of the inoculation area, a small hole was drilled into the skull. Then, 3×10^5 C6 cells in 3 μL were implanted into the left parietal cortex at a depth of 2 mm below the dura mater using a 10-μL, 26-gauge syringe (Hamilton). After a short incubation time, the syringe was slowly removed, the hole was closed with bone wax, and the skin was sutured. The well-being of the animals was monitored daily using a score sheet that included weight, behavior, posture, gait, and breathing rate.

Dual-Tracer Autoradiographic Studies with ^{18}F-Tracers and ^{131}I-SIP(L19)

Tracer uptake studies were performed 13–22 d after inoculation (based on preliminary MRI studies for tumor growth control; data not shown). One day before the autoradiographic experiments, 6–50 MBq of ^{131}I-SIP(L19) were administered via the tail vein to the conscious rats. The following day, a catheter was placed in the tail vein under isoflurane inhalation anesthesia, allowing intravenous application of 50–150 MBq of the ^{18}F-tracers. ^{18}F-Fluorocholine (*14*) and ^{18}F-FET (*15*) were injected 15 min, and ^{18}F-FDG 45 min, before removal of the brain (*16*). The animals were sacrificed using an overdose of intravenous pentobarbital. The brains were removed and instantly frozen in isopentane cooled to −50°C. For quantification of the ^{18}F tracers, 10-μm brain slices (100-μm slice distance) were placed on a phosphor imaging screen together with ^{14}C-standards and left for 240 min. Tritium-sensitive screens (Fuji TR2025) were used, because their uncoated, thin, sensitive layer yields higher-resolution ^{18}F-autoradiograms than do ordinary screens. After decay of the ^{18}F activity, the identical slices were again placed on the screens to get the ^{131}I-SIP(L19) autoradiograms. Both datasets were then scanned (Fuji BAS 1800 II; pixel size, 50 μm) and converted to kBq/cm^3. For this conversion, the ^{14}C-standards had previously been calibrated using a brain homogenate containing a defined amount of ^{18}F and ^{131}I.

For the quantitative analysis, the activities were decay-corrected to the time of screen exposure. Dividing these values by the amount of injected activity per gram of body weight yielded standardized uptake values (SUVs). Regions of interest were subsequently placed over the tumors and over the contralateral healthy cortex using the software PMOD (*17*). In addition, tumor uptake was divided by uptake in the contralateral cortex to obtain ratios of tumor to normal brain.

Morphologic Characterization

For morphologic analysis, the brain slices were fixed in 4% formalin/phosphate-buffered saline, followed by hematoxylin/eosin conventional staining and glial fibrillary acidic protein (GFAP) immunohistochemistry. In short, slides were incubated with anti-GFAP antibody (1:1000, DAKO Z0334) without pretreatment.

On adjacent slides, immunohistochemical labeling of the von-Willebrand factor was performed for visualization of blood vessels. Brain slices were pretreated with protease I for 4 min and stained with polyclonal antibody against von-Willebrand factor (1:1000, DAKO A00802). Finally, slides were developed using a Ventana machine and the iView DAB (DAKO) development kit.

Statistics

The corresponding autoradiographs were coregistered using the software PMOD. Regions of interest encompassing the whole tumor were then defined and applied to the ^{18}F tracers and ^{131}I-SIP(L19) autoradiographs. To investigate the correlation of the uptake pattern of each ^{18}F tracer with that of ^{131}I-SIP(L19), each 100th pixel was chosen for a regression analysis. Individual Pearson regression coefficients were then ż-transformed (Fisher's

ż-transformation) and averaged for the correlations ^{18}F-FDG vs. ^{131}I-SIP(L19), ^{18}F-fluorocholine vs. ^{131}I-SIP(L19), and ^{18}F-FET vs. ^{131}I-SIP(L19). These transformed average regression coefficients were compared pairwise according to Sachs (*18*) to assess differences in the correlations between each ^{18}F tracer and ^{131}I-SIP(L19).

RESULTS

Animals

No animal experienced tumor-induced side effects during the observation period.

Morphologic Characterization

The orthotopically grown tumors presented mostly in a compact glioblastomalike formation with or without necrosis (Fig. 1A). However, a subset of cells was found to invade the adjacent brain parenchyma or perivascular Virchow-Robin spaces (Figs. 1B and 1C). Immunohistochemical stains for GFAP revealed the astrocytic character of the tumor cells, although most did not express GFAP. The surrounding parenchyma presented with reactive, highly GFAP-positive astrocytes. Inflammatory cells such as lymphocytes or macrophages were not prominent. Transplanted tumor cells exhibited a homogeneous tumor mass with an evenly distributed microvascular network containing small arterioles and capillaries. A representative intratumoral microvessel stained against von-Willebrand factor is demonstrated in Figure 1D.

Tumoral Tracer Uptake

Examples of dual-tracer autoradiographs and corresponding correlations are demonstrated in Figures 2–4. In each tumor, the uptake of all tracers was substantially higher than in cortical gray matter. The uptake values are summarized in Table 1. ^{18}F-FDG displayed the highest SUV, followed by ^{18}F-FET, ^{18}F-fluorocholine, and ^{131}I-SIP(L19). Ratios of tumor to normal brain were highest for ^{131}I-SIP(L19), because of the low uptake in normal brain.

Correlation Between Uptake Pattern of ^{18}F-Tracers and ^{131}I-SIP(L19)

Regression analysis of tumor uptake of the ^{18}F-tracers and ^{131}I-SIP(L19) revealed the highest correlation for ^{18}F-fluorocholine ($\dot{z} = 0.80$, averaged ż-transformed Pearson correlation coefficient, $n = 6$), and ^{18}F-FET ($\dot{z} = 0.79$, $n = 6$). For ^{18}F-FDG, the correlation was poorer ($\dot{z} = 0.37$, $n = 5$). Pairwise comparison of the ż-transformed and averaged Pearson correlation coefficients revealed that ^{18}F-fluorocholine and ^{18}F-FET correlated significantly better with ^{131}I-SIP(L19) than did ^{18}F-FDG, whereas no significant difference was found in the correlations of ^{18}F-fluorocholine and ^{18}F-FET with ^{131}I-SIP(L19) (^{18}F-fluorocholine/^{131}I-SIP(L19) vs. ^{18}F-FDG/^{131}I-SIP(L19): $P < 0.01$, $\dot{z} = 2.98$; ^{18}F-FET/^{131}I-SIP(L19) vs. ^{18}F-FDG/^{131}I-SIP(L19): $P < 0.01$, $\dot{z} = 2.86$; ^{18}F-FET/^{131}I-SIP(L19) vs. ^{18}F-fluorocholine/^{131}I-SIP(L19): $P > 0.05$, $\dot{z} = 0.12$).

The order of the correlations is already evident in the autoradiographs depicted in Figures 2–4. The pattern of ^{18}F-fluorocholine and ^{18}F-FET uptake seems to correspond better with ^{131}I-SIP(L19) uptake (Figs. 2 and 3) than did the pattern of ^{18}F-FDG uptake (Fig. 4).

DISCUSSION

The oncofetal domain, the so-called extra domain B, of fibronectin is one of the few markers of angiogenic processes known thus far and has frequently been studied in the past 2 decades (*1*). Because malignant tumor growth is often characterized by an increased development of new blood vessels, angiogenic markers seem promising for

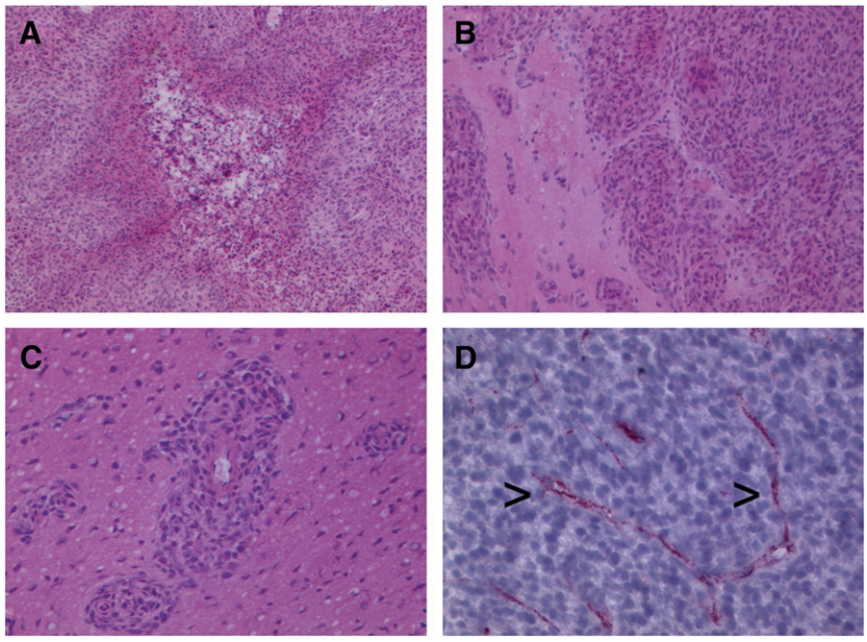

FIGURE 1. Morphologic characterization of transplanted glioma cells and developing tumor: central necrotic area (hematoxylin/eosin, ×60) (A), parenchymal infiltration zone of glioma cells (hematoxylin/eosin, ×100) (B), infiltration in Virchow-Robin perivascular space (hematoxylin/eosin, ×130) (C), and representative intratumoral microvessels (arrowheads; anti–von-Willebrand factor, ×200) (D).

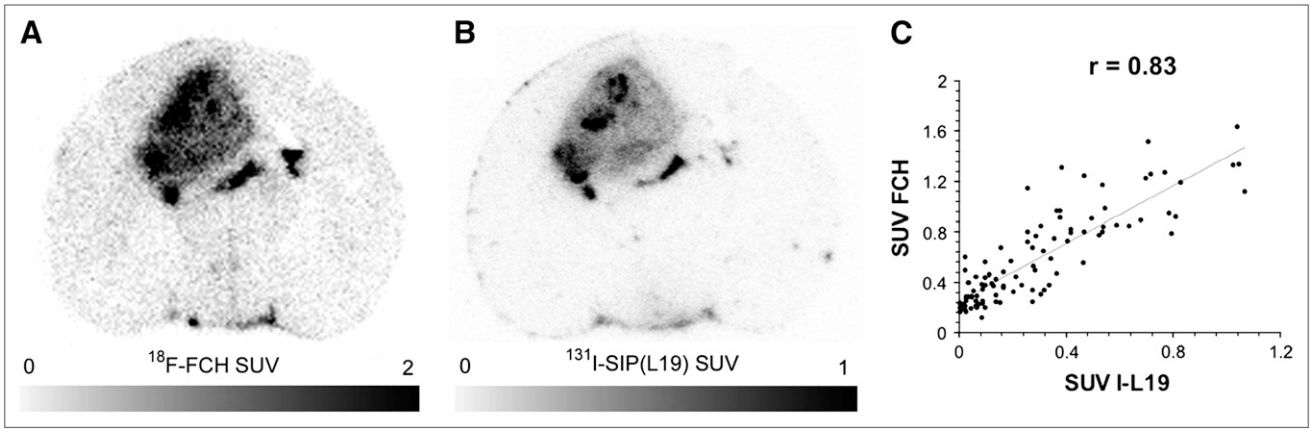

FIGURE 2. (A and B) Dual-tracer autoradiographs of ^{18}F-fluorocholine (FCH) (A) and corresponding ^{131}I-SIP(L19) (B). (C) Pixelwise correlation of each 100th pixel in tumor region of interest and Pearson correlation coefficient.

tumor diagnosis therapy and therapy evaluation (*1,2*). During the last few years, immunoconjugates such as SIP(L19), with promising characteristics regarding molecular stability, clearance rate, and tumor accumulation (*5,7*), have been introduced in clinical research. Santimaria et al. and Castellani et al. demonstrated the potential of L19 antibodies for brain tumor diagnosis (*6,8*). Encouraged by these studies, we investigated uptake of ^{131}I-SIP(L19) in an orthotopically inoculated C6 rat glioma model and compared the results with three ^{18}F-labeled established oncologic PET tracers.

C6 Rat Glioma Model

The C6 rat glioma model adequately reflects the growth and invasion of the human glioblastoma (*19*). The implantation of the tumor cells into animal brain tissue as performed in the present study closely mimics the natural behavior of brain tumors and, unlike simpler models (e.g., subcutaneous tumor models), has the advantage of activating vascular mechanisms. Accordingly, we found morphologic characteristics similar to those present in human glioblastomas. For instance, a high tendency to infiltrate the adjacent brain tissue and areas of necrosis could be detected (Fig. 1). These findings support the relevance of our results to PET of human glioma patients.

Tumor Tracer Uptake

Of all the ^{18}F tracers, ^{18}F-FDG displayed the highest tumor SUV, followed by ^{18}F-FET and ^{18}F-fluorocholine. This order is similar to the one we found in another cell line (F98 gliomas), although the SUV for all tracers was somewhat higher in the F98 gliomas (*10*). Because of the low accumulation in normal brain tissue, ^{18}F-fluorocholine displayed the highest tumor-to-cortex ratio of the ^{18}F tracers.

The highest tumor-to-cortex ratio was achieved with ^{131}I-SIP(L19), although an exact value cannot be indicated because the uptake in normal cortex was so low it could not adequately be measured. Nevertheless, the high tumor-to-cortex ratio is evident in Figures 2B, 3B, and 4B. This high tumor-to-cortex ratio opens the possibility of using iodine-labeled SIP(L19) for the work-up of brain tumor patients. A promising application might be the differentiation of tumor recurrence from postoperative changes or radiation injury. For this purpose, the value of ^{18}F-FET and other amino acid analogs and also ^{18}F-FDG has already been established

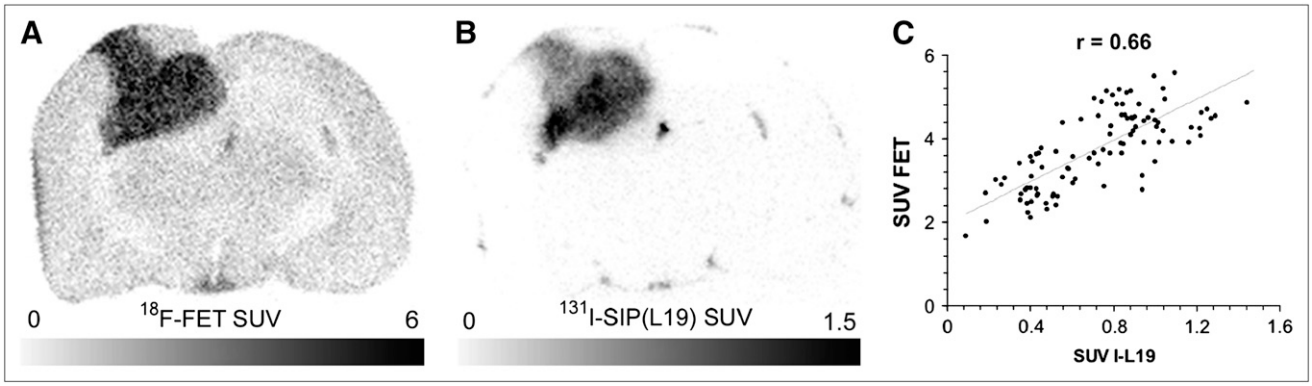

FIGURE 3. (A and B) Dual-tracer autoradiographs of ^{18}F-FET (A) and corresponding ^{131}I-SIP(L19) (B). (C) Pixelwise correlation of each 100th pixel in tumor region of interest and Pearson correlation coefficient.

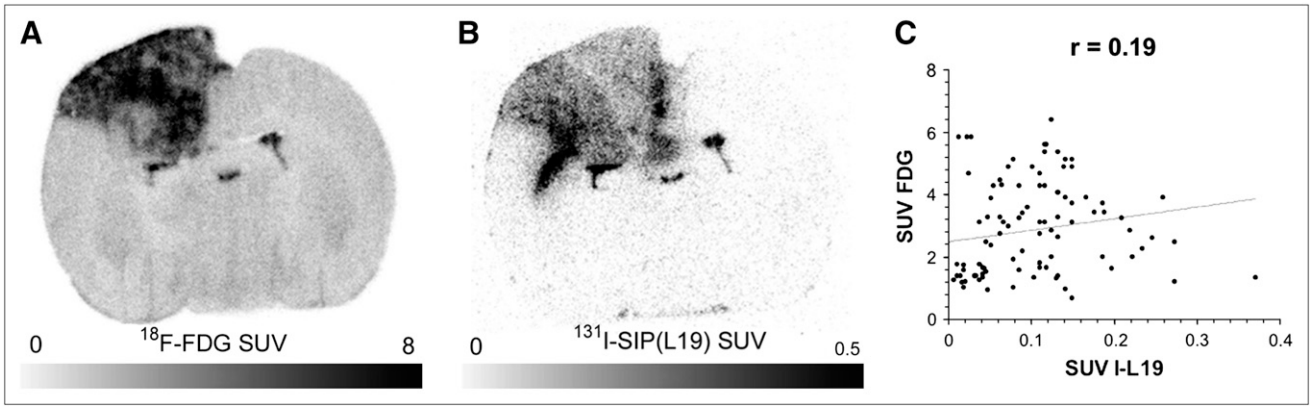

FIGURE 4. (A and B) Dual-tracer autoradiographs of ^{18}F-FDG (A) and corresponding ^{131}I-SIP(L19) (B). (C) Pixelwise correlation of each 100th pixel in tumor region of interest and the Pearson correlation coefficient.

(*12,20–23*). Furthermore, SIP(L19) labeled with ^{131}I or ^{123}I opens the opportunity of using SPECT, which is more widely available than PET and potentially less expensive.

Another application of ^{131}I-SIP(L19) is radioimmunotherapy of brain tumors. In animal models, such an approach has proven promising. Using the same C6 cell line, radioimmunotherapy with ^{131}I-SIP(L19) seemed to prolong survival (*24*). A similar result was published in a study on mice bearing head and neck cancer xenografts (*25*).

TABLE 1
SUVs in Animals with Induced C6 Gliomas

Animal	Tracer	Tumor	CTX	Tumor/CTX	^{131}I-SIP(L19) tumor
1	^{18}F-fluorocholine	2.43	0.48	5.06	0.40
2	^{18}F-fluorocholine	1.90	0.46	4.13	0.26
3	^{18}F-fluorocholine	2.24	0.62	3.61	0.40
4	^{18}F-fluorocholine	1.69	0.42	4.02	0.57
5	^{18}F-fluorocholine	2.57	0.50	5.14	0.67
6	^{18}F-fluorocholine	1.14	0.44	2.59	0.11
Mean		2.00	0.49	4.09	0.40
SD		0.53	0.07	0.95	0.20
7	^{18}F-FET	4.24	1.57	2.70	0.34
8	^{18}F-FET	3.50	1.65	2.12	0.37
9	^{18}F-FET	3.43	1.04	3.30	0.04
10	^{18}F-FET	3.26	1.51	2.16	0.23
11	^{18}F-FET	3.67	1.36	2.70	0.8
12	^{18}F-FET	3.94	1.36	2.90	0.46
Mean		3.67	1.42	2.65	0.37
SD		0.36	0.22	0.45	0.25
13	^{18}F-FDG	7.97	4.38	1.82	0.07
14	^{18}F-FDG	5.31	3.08	1.72	0.17
15	^{18}F-FDG	7.20	3.60	2.00	0.28
16	^{18}F-FDG	7.14	3.84	1.86	0.04
17	^{18}F-FDG	8.54	3.28	2.60	0.14
Mean		7.23	3.64	2.00	0.14
SD		1.22	0.51	0.35	0.09

Tumor = area of average SUV in tumor; CTX = contralateral cortex.

Correlation of Pixelwise Uptake of ^{18}F Tracers and ^{131}I-SIP(L19)

Pixelwise correlation of each ^{18}F tracer and ^{131}I-SIP(L19) uptake revealed higher correlation coefficients for ^{18}F-fluorocholine and ^{18}F-FET than for ^{18}F-FDG. These findings may be explained by the different metabolic pathways.

^{18}F-Fluorocholine is a choline analog and has uptake characteristics similar to those of radiolabeled natural choline (*11,26*). Choline, an essential compound of the cell membrane, is transported into mammalian cells and then phosphorylated by choline kinase (*27*). In a further step, it is metabolized to phosphatidylcholine, which is incorporated into the cell membrane. In previous studies, the increased choline uptake in tumor cells was explained mainly by the upregulation of choline kinase due to an increased demand of membrane constituents (*28,29*). Consequently, further in vitro and in vivo studies postulated the use of choline analogs as a marker for tumor proliferation (*9,29,30*). Because ^{18}F-fluorocholine mimics natural choline, it might be a potential tracer of proliferation, too. This possibility with regard to brain tumors has not yet been adequately explored. There have been only anecdotal investigations of ^{18}F-fluorocholine uptake in human brain tumors (*14,31,32*). The positive correlation between ^{18}F-fluorocholine and ^{131}I-SIP(L19) may be due to several factors. Neither tracer penetrates an intact blood–brain barrier. Therefore, disruption of the latter in the neoangiogenic vessels may increase leakage of both tracers to a similar degree. However, this is not likely to be the main reason, because our previous results did not demonstrate an effect of the degree of brain barrier disruption on ^{18}F-fluorocholine uptake in F98 glioma cells (*10*). Another, more likely, possibility is that a combination of increased blood flow and blood–brain barrier disruption leads to the positive correlation.

The amino acid analog ^{18}F-FET is taken up by a specific amino acid carrier (L-system) located in the tumor cell membrane but is not metabolized or incorporated into proteins (*33,34*). In brain tumors, ^{18}F-FET has to cross

the blood–brain barrier via endothelial L-transporters or diffusion through the impaired blood–brain barrier of tumor vessels (*10,12,35*). The latter mechanism can also be assumed to be the main route of ^{131}I-SIP(L19) into tumors after intravenous application and may thus explain the positive correlation between these tracers in our study. This explanation is in line with our previous study (*10*), which demonstrated a trend toward a positive correlation between ^{18}F-FET uptake and the degree of blood–brain barrier disruption. In contrast to ^{18}F-fluorocholine, ^{18}F-FET as evaluated by SUVs does not seem to have the same potential for the grading of brain tumors (*22,36,37*). It remains to be confirmed that the kinetics of ^{18}F-FET may allow some degree of grading (*38*). Nevertheless, the still decent correlation of ^{18}F-FET uptake with that of ^{131}I-SIP(L19) suggests that ^{18}F-FET may also be useful for the assessment of treatment response to antiangiogenic therapy.

Finally, ^{18}F-FDG, the most widely used tracer in oncologic PET today, is taken up into cells by glucose transporters and then phosphorylated by the enzyme hexokinase, the first enzyme of glycolysis. Both glucose transporter expression and hexokinase activity are upregulated in tumor cells (*39*), as explains the differential uptake of ^{18}F-FDG in different tumors. In addition, the ^{18}F-FDG uptake is not substantially affected by perfusion or disruption of the blood–brain barrier (*10,40*). This suggestion is in accordance with our findings and may explain the poor correlation between ^{18}F-FDG and ^{131}I-SIP(L19) uptake, although we cannot exclude that the relatively low ^{131}I-SIP(L19) uptake in the ^{18}F-FDG group contributes to the worse correlation. The lower mean ^{131}I-SIP(L19) uptake in the ^{18}F-FDG group itself is probably coincidental, because we found no specific reason.

An interesting question concerns the suitability of the investigated ^{18}F-tracers for monitoring antiangiogenic therapy. Does the higher correlation of ^{18}F-fluorocholine and ^{18}F-FET with ^{131}I-SIP(L19) indicate that these tracers are more suitable than ^{18}F-FDG for that purpose? This possibility would be an interesting subject of future studies. In such studies, the change of tracer uptake after antiangiogenic treatment could be correlated with long-term outcome.

Comparison of ^{18}F Tracer Uptake in C6 and F98 Glioma

In a previous study, we used the same methodology to measure the uptake of the same ^{18}F tracers in rats bearing F98 gliomas (*10*). It is interesting to note that the mean ^{18}F-FDG and ^{18}F-fluorocholine uptakes were substantially higher (52% and 49%, respectively) in the biologically more aggressive F98 cell line whereas ^{18}F-FET uptake was only 14% higher. This result suggests that ^{18}F-fluorocholine, like ^{18}F-FDG, may also be useful for grading brain tumors, whereas ^{18}F-FET seems less suitable for that purpose. This suggestion is in line with the finding of previous studies demonstrating that ^{18}F-FET SUV was not suitable for tumor grading (*22,36,37*).

CONCLUSION

One day after intravenous injection, ^{131}I-SIP(L19) displayed a high tumor-to-cortex ratio, which may be used in the diagnostic work-up of brain tumor patients. Of the 3 investigated ^{18}F tracers, ^{18}F-fluorocholine and ^{18}F-FET correlated better with the pattern of ^{131}I-SIP(L19) uptake than did ^{18}F-FDG. Whether this means that ^{18}F-fluorocholine and ^{18}F-FET are better suited than ^{18}F-FDG for monitoring antiangiogenic treatment should be investigated in future studies.

ACKNOWLEDGMENTS

This study was supported by the Wilhelm-Sander-Stiftung in Zurich. The authors thank Tibor Cservényak and Konstantin Drandarov for tracer production, Kerstin Goepfert and Amélie Lutz for technical assistance with MRI, and Florent Haiss for important laboratory work. Furthermore we appreciate the valuable discussions with Gustav K. von Schulthess and Gerrit Westera. Three of the authors were supported by the Swiss National Science Foundation.

REFERENCES

1. Neri D, Bicknell R. Tumour vascular targeting. *Nat Rev Cancer.* 2005;5: 436–446.
2. Folkman J. Tumor angiogenesis: therapeutic implications. *N Engl J Med.* 1971; 285:1182–1186.
3. Zardi L, Carnemolla B, Siri A, et al. Transformed human cells produce a new fibronectin isoform by preferential alternative splicing of a previously unobserved exon. *EMBO J.* 1987;6:2337–2342.
4. Pini A, Viti F, Santucci A, et al. Design and use of a phage display library: human antibodies with subnanomolar affinity against a marker of angiogenesis eluted from a two-dimensional gel. *J Biol Chem.* 1998;273:21769–21776.
5. Borsi L, Balza E, Bestagno M, et al. Selective targeting of tumoral vasculature: comparison of different formats of an antibody (L19) to the ED-B domain of fibronectin. *Int J Cancer.* 2002;102:75–85.
6. Santimaria M, Moscatelli G, Viale GL, et al. Immunoscintigraphic detection of the ED-B domain of fibronectin, a marker of angiogenesis, in patients with cancer. *Clin Cancer Res.* 2003;9:571–579.
7. Berndorff D, Borkowski S, Sieger S, et al. Radioimmunotherapy of solid tumors by targeting extra domain B fibronectin: identification of the best-suited radioimmunoconjugate. *Clin Cancer Res.* 2005;11:7053s–7063s.
8. Castellani P, Borsi L, Carnemolla B, et al. Differentiation between high- and low-grade astrocytoma using a human recombinant antibody to the extra domain-B of fibronectin. *Am J Pathol.* 2002;161:1695–1700.
9. Kaim AH, Weber B, Kurrer MO, et al. ^{18}F-FDG and ^{18}F-FET uptake in experimental soft tissue infection. *Eur J Nucl Med Mol Imaging.* 2002;29: 648–654.
10. Spaeth N, Wyss MT, Pahnke J, et al. Uptake of ^{18}F-fluorocholine, ^{18}F-fluoroethyl-L: -tyrosine and ^{18}F-fluoro-2-deoxyglucose in F98 gliomas in the rat. *Eur J Nucl Med Mol Imaging.* 2006;33:673–682.
11. DeGrado TR, Baldwin SW, Wang S, et al. Synthesis and evaluation of ^{18}F-labeled choline analogs as oncologic PET tracers. *J Nucl Med.* 2001;42: 1805–1814.
12. Spaeth N, Wyss MT, Weber B, et al. Uptake of ^{18}F-fluorocholine, ^{18}F-fluoroethyl-L-tyrosine, and ^{18}F-FDG in acute cerebral radiation injury in the rat: implications for separation of radiation necrosis from tumor recurrence. *J Nucl Med.* 2004;45:1931–1938.
13. Ambar BB, Frei K, Malipiero U, et al. Treatment of experimental glioma by administration of adenoviral vectors expressing Fas ligand. *Hum Gene Ther.* 1999;10:1641–1648.
14. DeGrado TR, Coleman RE, Wang S, et al. Synthesis and evaluation of ^{18}F-labeled choline as an oncologic tracer for positron emission tomography: initial findings in prostate cancer. *Cancer Res.* 2001;61:110–117.

15. Weber WA, Wester HJ, Grosu AL, et al. O-(2-[^{18}F]fluoroethyl)-L-tyrosine and L-[methyl-^{11}C]methionine uptake in brain tumours: initial results of a comparative study. *Eur J Nucl Med.* 2000;27:542–549.
16. Huang SC, Phelps ME, Hoffman EJ, et al. Noninvasive determination of local cerebral metabolic rate of glucose in man. *Am J Physiol.* 1980;238:E69–E82.
17. Mikolajczyk K, Szabatin M, Rudnicki P, Grodzki M, Burger CA. JAVA environment for medical image data analysis: initial application for brain PET quantitation. *Med Inform (Lond).* 1998;23:207–214.
18. Sachs L. *Angewandte Statistik.* Berlin, Germany: Springer-Verlag; 1997.
19. Grobben B, De Deyn PP, Slegers H. Rat C6 glioma as experimental model system for the study of glioblastoma growth and invasion. *Cell Tissue Res.* 2002; 310:257–270.
20. Chao ST, Suh JH, Raja S, Lee SY, Barnett G. The sensitivity and specificity of FDG PET in distinguishing recurrent brain tumor from radionecrosis in patients treated with stereotactic radiosurgery. *Int J Cancer.* 2001;96:191–197.
21. Langleben DD, Segall GM. PET in differentiation of recurrent brain tumor from radiation injury. *J Nucl Med.* 2000;41:1861–1867.
22. Popperl G, Gotz C, Rachinger W, et al. Value of O-(2-[^{18}F]fluoroethyl)-L-tyrosine PET for the diagnosis of recurrent glioma. *Eur J Nucl Med Mol Imaging.* 2004;31:1464–1470.
23. Tsuyuguchi N, Sunada I, Iwai Y, et al. Methionine positron emission tomography of recurrent metastatic brain tumor and radiation necrosis after stereotactic radiosurgery: is a differential diagnosis possible? *J Neurosurg.* 2003;98:1056–1064.
24. Spaeth N, Wyss MT, Pahnke J, et al. Radioimmunotherapy targeting the extra domain B of fibronectin in C6 rat gliomas: a preliminary study about the therapeutic efficacy of iodine-131-labeled SIP(L19). *Nucl Med Biol.* 2006;33:661–666.
25. Tijink BM, Neri D, Leemans CR, et al. Radioimmunotherapy of head and neck cancer xenografts using ^{131}I-labeled antibody L19-SIP for selective targeting of tumor vasculature. *J Nucl Med.* 2006;47:1127–1135.
26. Hara T. ^{11}C-Choline and 2-deoxy-2-[^{18}F]fluoro-D-glucose in tumor imaging with positron emission tomography. *Mol Imaging Biol.* 2002;4:267–273.
27. Hernandez-Alcoceba R, Saniger L, Campos J, et al. Choline kinase inhibitors as a novel approach for antiproliferative drug design. *Oncogene.* 1997;15:2289–2301.
28. Katz-Brull R, Degani H. Kinetics of choline transport and phosphorylation in human breast cancer cells: NMR application of the zero trans method. *Anticancer Res.* 1996;16:1375–1380.
29. Yoshimoto M, Waki A, Obata A, et al. Radiolabeled choline as a proliferation marker: comparison with radiolabeled acetate. *Nucl Med Biol.* 2004;31:859–865.
30. Al-Saeedi F, Welch AE, Smith TA. [methyl-^{3}H]Choline incorporation into MCF7 tumour cells: correlation with proliferation. *Eur J Nucl Med Mol Imaging.* 2005;32:660–667.
31. Kwee SA, Coel MN, Lim J, Ko JP. Combined use of F-18 fluorocholine positron emission tomography and magnetic resonance spectroscopy for brain tumor evaluation. *J Neuroimaging.* 2004;14:285–289.
32. Hara T, Kondo T, Kosaka N. Use of ^{18}F-choline and ^{11}C-choline as contrast agents in positron emission tomography imaging-guided stereotactic biopsy sampling of gliomas. *J Neurosurg.* 2003;99:474–479.
33. Wester HJ, Herz M, Weber W, et al. Synthesis and radiopharmacology of O-(2-[^{18}F]fluoroethyl)-L-tyrosine for tumor imaging. *J Nucl Med.* 1999;40:205–212.
34. Langen KJ, Jarosch M, Muhlensiepen H, et al. Comparison of fluorotyrosines and methionine uptake in F98 rat gliomas. *Nucl Med Biol.* 2003;30:501–508.
35. Duelli R, Enerson BE, Gerhart DZ, Drewes LR. Expression of large amino acid transporter LAT1 in rat brain endothelium. *J Cereb Blood Flow Metab.* 2000; 20:1557–1562.
36. Cheon GJ, Ahn SH, Cho YS, et al. Correlation of ^{18}F-FET uptake and histologic grades of primary brain tumors [abstract]. *J Nucl Med.* 2003;44(suppl):367P.
37. Pauleit D, Floeth F, Hamacher K, et al. O-(2-[^{18}F]fluoroethyl)-L-tyrosine PET combined with MRI improves the diagnostic assessment of cerebral gliomas. *Brain.* 2005;128:678–687.
38. Weckesser M, Langen KJ, Rickert CH, et al. O-(2-[(18)F]fluorethyl)-L-tyrosine PET in the clinical evaluation of primary brain tumours. *Eur J Nucl Med Mol Imaging.* 2005;32:422–429.
39. Gambhir SS. Molecular imaging of cancer with positron emission tomography. *Nat Rev Cancer.* 2002;2:683–693.
40. Pugachev A, Ruan S, Carlin S, et al. Dependence of FDG uptake on tumor microenvironment. *Int J Radiat Oncol Biol Phys.* 2005;62:545–553.